(CONF-752918--1

MECHANICAL AND PHYSICAL PROPERTIES OF 2 1/4 Cr-1 Mo STEEL IN SUPPORT OF CRBRP STEAM GENERATOR DESIGN*

C. R. Brinkman, R. K. Williams, R. L. Klueh, and T. L. Hebble

Paper to be Presented at
the International Conference on
Materials for Nuclear Steam Generators
Gatlinburg, Tennessee
Sept. 9–12, 1975

Submitted to Nuclear Technology

Oak Ridge National Laboratory
P.O. Box X
Oak Ridge, Tennessee 37830
615-483-8611 Ext. 3-6038

*Research sponsored by the U.S. Energy Research and Development Administration under contract with Union Carbide Corporation.

MECHANICAL AND PHYSICAL PROPERTIES OF 2 1/4 Cr-1 Mo STEEL IN SUPPORT OF CRBRP STEAM GENERATOR DESIGN

C. R. Brinkman, R. K. Williams, R. L. Klueh, and T. L. Hebble
Oak Ridge National Laboratory
Oak Ridge, Tennessee 37830

Mechanical and physical property tests on annealed 2 1/4 Cr-1 Mo steel were conducted in an effort to define behavior in support of the design of the Clinch River Breeder Reactor Plant (CRBRP) steam generator design. Interim empirical expressions and/or data are reported from the results of tensile, creep, fatigue, creep-fatigue, subcritical crack growth, thermal conductivity, thermal diffusivity, and thermal expansion tests and analysis. These expressions cover behavior, where appropriate, over a range of temperatures from 25 to as high as 700°C. Comparisons between thermal conductivity and diffusivity values and those found in the American Society of Mechanical Engineers (ASME) Code indicated that the new values were significantly higher than those found presently in the Code. The importance and complexity of obtaining valid mechanical and physical properties for the Clinch River Breeder Reactor Plant (CRBRP) steam generator are discussed.

INTRODUCTION

Design of steam generators for the Clinch River Breeder Reactor Plant (CRBRP) requires an extensive knowledge of both physical and mechanical properties in order to follow the design guidelines and procedures established for Class I Components in Section III of the American Society of Mechanical Engineers (ASME) Boiler and Pressure Vessel Code. However, additional information concerning material performance is required in order to develop constitutive equations for inelastic analysis. Material studies must produce information concerning fabricability, weldability, and variability of properties

for a specified material resulting from minor variations in composition, melting practice, and thermomechanical processing history from heat-to-heat. Finally, data are required to quantify potential long-term degradation from other factors such as metallurgical instability resulting from thermal aging (1) and environmental effects (2). Consider a partial list of some of the more important physical and mechanical property tests in Table I. These tests must be performed at appropriate temperatures and strain rates and, when applicable, with additional tests for environmental and metallurgical stability. Such an undertaking requires well thought out and coordinated interdisciplinary materials investigations, which are currently under way in several laboratories in the United States. For CRBRP steam generator development, first attention is being directed at understanding the behavior of 2 1/4 Cr-1 Mo steel (annealed) as the base material, with associated weldment filler metals for transition joints such as Inconel 82 and type 16-8-2 stainless steel (Fe–16% Cr–8% Ni–2% Mo).

While both mechanical and physcial property tests are currently under way on all these materials, only the base material 2 1/4 Cr-1 Mo steel behavior will be discussed. It was the objective of this paper, therefore, to present recent results of some of the experimental tests and analytically developed mathematical descriptions aimed at characterizing the mechanical and physical properties of 2 1/4 Cr-1 Mo steel.

MECHANICAL PROPERTIES

Because of the complexity of mechanical data and the limitations of space, only representative indications of mechanical behavior defined by the tests in Table I will be discussed herein. Additional results from this effort can be found elsewhere (3–5).

Tensile Properties

An extensive tensile testing program was conducted in order to obtain tensile properties from a given heat of material for comparison with previously obtained data and to provide some of the data base required for establishment of interim constitutive equations for this material.

The tensile studies to be described were conducted on a single heat of commercial 2 1/4 Cr-1 Mo steel, which was in the form of a 25.4-mm-thick plate obtained from Babcock and Wilcox Company (B&W heat 20017). The chemical composition is given in Table II. Tests were conducted on this heat in the annealed condition: 1 hr at 927°C, then furnace cooled. The microstructure of the material was primarily proeutectoid ferrite with small amounts of pearlite and bainite.

Tests were conducted over the range 25 to 593°C and at strain rates of 2.67×10^{-6} to 144/sec. Therefore, the variation in tensile properties with strain rate could be described over eight orders of magnitude (4,5).

Figures 1 to 4 show the three-dimenstional representations of the 0.2% offset yield stress, ultimate tensile strength, total elongation, and reduction of area over strain rates of 2.7×10^{-6} to 144/sec and from 25 to 566°C. With two exceptions, the topography of the yield-stress strain-rate temperature surface was quite smooth (Fig. 1). The only exceptions were a minor peak at about 371°C and 0.16/sec and a rather large increase in yield strength with increasing strain rate and decreasing temperature as the high-strain-rate room-temperature corner was approached.

The ultimate-tensile-strength strain-rate temperature relationship shown in Fig. 2 was much more complex. As with the yield strength, there was a large increase in the ultimate tensile strength in the high-strain-rate low-temperature corner. The main distinguishing feature of the topography, however, is the

ridge that has its peak at about 371°C and 2.7×10^{-6}/sec (the lowest strain rate) and extends diagonally downward toward the high-strain-rate high-temperature corner. At 144/sec, the highest strain rate tested, the peak occurred near 566°C. Note also that, although the peak strength occurred at the lowest strain rate at about 371°C, the strength at this strain rate rapidly decreased as the temperature was increased.

Strain rate effects on the ultimate tensile strength can be broken into two types, both of which occur in this steel. Normally, strength decreases with decreasing strain rate and increasing temperature, conditions that promote recovery during testing. This is the reason for the large drop in ultimate tensile strength at the low-strain-rate high-temperature corner of Fig. 2. The second effect, dynamic strain aging, strengthens the steel and gives rise to the ridge in Fig. 2. Dynamic strain aging is the result of interactions of solute atoms (e.g., carbon and nitrogen) with dislocations. The increase in the temperature at which the peak strength occurs with increasing strain rate is a reflection of the increased diffusion rate of the solutes with increased temperature (i.e., at the highest temperatures for the high strain rate, the solutes that led to dislocation locking can diffuse rapidly enough to enhance the strength).

The effect of strain rate on total elongation, Fig. 3, tends to be the inverse of the effect on tensile strength. The behavior of the reduction of area, Fig. 4, paralleled that for the total elongation.

To determine the best empirical analytical representation of the stress-strain behavior of annealed 2 1/4 Cr-1 Mo steel, the true-stress true-plastic-strain data between the 0.2% offset yield stress and the ultimate tensile strength for tests between 25 and 593°c and 2.7×10^{-3}/sec were fit with a model proposed by Voce (6).

The Voce equation is a three-parameter equation,

$$\sigma = A_4 \exp(C_4\varepsilon_p) + B_4 \ , \tag{1}$$

where σ is the true stress, ε_p the true plastic strain, and A_4, B_4, and C_4 are material constants. For strain rates of 6.7×10^{-3} to 6.7×10^{-5}/sec, the equation for the upper limit, ε_p^{max}, was obtained by fitting a straight line to the uniform elongation data:

$$\varepsilon_p^{max} = \ln(1.133 - 0.000104T_c) \ , \tag{2}$$

where T_c is temperature in °C. Although the lowest measured value of ε_p fit to Eq. (1) was 0.002, the extrapolated values at $\varepsilon_p = 0.001$ were in good agreement with the original true-stress true-plastic-strain curves. Below $\varepsilon_p \approx 0.001$, the observed stresses decrease more rapidly than predicted by Eq. (1). A comparison of the proportional limits ($\varepsilon_p = 0$) estimated from the load strain charts with those obtained from Eq. (1) indicated that the estimated values for stress are 10 to 20% high.

In Figs. 5, 6, and 7, A_4, B_4, and C_4 are shown as functions of temperature. All three constants show a dependence on strain rate and are nonmonotonic functions of temperature. Since A_4 and B_4 define the magnitude of the stress, it is not unreasonable to expect a relationship between these constants and strength. Indeed, A_4 and B_4 were found to be linear functions of the ultimate tensile strength, τ:

$$A_4 = -1.059\tau + 27.49 \ , \tag{3}$$

and

$$B_4 = 1.231\tau - 6.954 \ , \tag{4}$$

where A_4, B_4, and τ are in ksi (1 ksi = 6.895 MPa). Note that one relationship fits all temperatures and strain rates. (Linear relationships were also found with the yield strength.) Hence, if the ultimate tensile strength is known, both A_4 and B_4 can be determined. As expected, no relationship between C_4 and τ was evident. When C_4 was plotted against the uniform elongation, however, a nonlinear relationship that appeared independent of strain rate was obtained.

Knowing how tensile properties for a single heat of annealed 2 1/4 Cr-1 Mo steel vary as a function of temperature and strain rate, one might like to know the range of values possible due to slight variations in composition, product form, etc. In Fig. 8 values of yield strength are plotted as a function of temperature. The data represent the results of a large number of tests conducted at our laboratory and elsewhere on 2 1/4 Cr-1 Mo steel in the annealed or isothermally annealed condition. Data shown are from tests conducted on several product forms including tube and pipe, bar and rod, and plate made of material conforming to the following ranges of composition and room-temperatures mechanical properties:

Carbon content: 0.07–0.15 wt %
Chromium content: 2.0–2.5 wt %
Molybdenum content: 0.9–1.1 wt %
Minimum room temperature ultimate tensile strength:
60 ksi (414 MPa)
Minimum room temperature (0.2% offset) yield strength:
30 ksi (207 MPa)

Upper, lower, and expected values are indicated by the solid line through the data. The upper and lower lines represent the (P = 0.90, λ = 0.95) tolerance limits; that is, at a confidence level of 0.95; 95% of the observed values are expected to be greater than the lower limit.

Creep Properties

Using the results of 37 creep tests from several laboratories over the temperature range of 454 to 593°C for test times up to 5000 hr, a creep equation was formulated (3). The equation is considered to be valid for annealed material exhibiting clearly defined primary and secondary stages in the creep curve and having room-temperature ultimate tensile strengths between 70 and 75 ksi (483 and 517 MPa), yield strengths at least 30 ksi (207 MPa), and the composition limitations 0.07–0.15 wt % C, 2.0–2.5 wt % Cr, and 0.9–1.1 wt % Mo. The equation may be expressed as:

$$\varepsilon_c = \frac{t}{A + Bt} + \dot{\varepsilon}_m t \ , \qquad (5)$$

where ε_c = creep strain (%),

t = time (hr),

$\dot{\varepsilon}_m$ = minimum creep rate (%/hr),

and A, B, and $\dot{\varepsilon}_m$ depend upon stress and temperature as follows:

$$\log A = 12.26 - 3.348 \times 10^{-6}T^2 + 9.353 \times 10^{-4}\sigma^2 - 1.167 \times 10^{-4}T \ ,$$

$$\log B = -52.19 + 8.682 \times 10^{-2}T - 3.368 \times 10^{-5}T^2 - 1.152(\log \sigma)^2 \ ,$$

$$\log \dot{\varepsilon}_m = -30.04 + 1.516 \times 10^{-2}T + 2.001 \times 10^{-3}T(\log \sigma)^2 \ ,$$

where σ = stress (ksi) and T = temperature (°F + 460).

The above model is expected to predict reasonable values of creep strain for annealed material in the following stress, temperature, and time regions:

1 ksi (7 MPa) $\leq \sigma \leq$ 65 ksi (448 MPa) ultimate tensile strength,

700°F (371°C) $\leq T \leq$ 1100°F (593°C),

$T <$ time to tertiary creep.

An interim empirical equation for predicting the onset of tertiary creep was then developed and is as follows:

$$\log t_3 = b_0 + b_1 \log \sigma + b_2 T + b_3 (10)^{(T \log \sigma)/1000} , \qquad (6)$$

where t_3 = time to tertiary creep (hr),

σ = stress (Mpa or ksi),

T = temperature (K or °R), K = °C + 273, °R = °F + 460.

Table III lists the coefficients found for Eq. (6) and their standard errors. The stress and temperature ranges over which the model predicts reasonable and consistent results are 644 K (1160°R) $\leq T \leq$ 866 K (1560°R), $\sigma <$ 276 MPa (40 ksi), $t <$ 50,000 hr. Additional information concerning the creep behavior of this material can be found elsewhere (3,7).

Fatigue Properties

Fatigue analysis is an important consideration in the design of reactor components that are subject to thermal transients. At the onset of this investigation there was not a valid set of elevated-temperature ASME Code approved fatigue curves for 2 1/4 Cr-1 Mo steel. Therefore, a concerted effort was directed at obtaining new and collecting literature fatigue data to establish valid fatigue curves. Fully reversed load- and strain-controlled fatigue tests were conducted over the range from room temperature to 593°C (8). Fatigue curves below 315°C plotted at each temperature (9) were compared, and temperature had little or no effect on low-cycle fatigue resistance. However, in the high-cycle region (i.e., $>10^5$ cycles to failure) the fatigue resistance of this material was actually greater at 315°C than it was at room temperature. This was attributed to dynamic strain aging. To avoid crossover complications and because of the minimal overall reduction in fatigue life attributable to temperature effects alone up to 427°C, we decided to construct only three fatigue design curves beginning at 427°C. The design curves were established as follows:

Using conventional ASME practice, average curves were derived for the data at 427, 482–538, and 593°C. Lower limit design curves were then obtained by taking the lesser of safety factors of 2 on strain range and 20 on cycles to failure (10) graphically smoothing the result into a single curve. This last curve was then fit by a fourth degree polynomial in ln N_f. The final design curves shown in Fig. 9 were calculated from the polynomial equations, which are:

$$[427°C] \quad \ln \Delta\varepsilon_t = 7.103 \times 10^{-5}(\ln N_d)^4 - 4.246 \times 10^{-3}(\ln N_d)^3 + 8.995 \times 10^{-3}(\ln N_d)^2 - 1.173(\ln N_d) - 0.5925 , \tag{7}$$

$$[482–538°C] \quad \ln \Delta\varepsilon_t = 1.299 \times 10^{-4}(\ln N_d)^4 - 6.852 \times 10^{-3}(\ln N_d)^3 + 0.137(\ln N_d)^2 - 1.391(\ln N_d) - 0.369 , \tag{8}$$

$$[593°C] \quad \ln \Delta\varepsilon_t = 7.007 \times 10^{-5}(\ln N_d)^4 - 3.910 \times 10^{-3}(\ln N_d)^3 + 8.821 \times 10^{-2}(\ln N_d)^2 - 10.59(\ln N_d) - 1.256 , \tag{9}$$

where $\Delta\varepsilon_t$ is the total strain range and N_d is the design cyclic life time. The above proposed design curves are considered to be valid in air over the range shown (10 to 10^8 cycles) and for strain rates equal to or in excess of 4×10^{-3}/sec. However, these curves do not take into account dynamic strain aging, creep-fatigue, or environmental interaction other than in air. In an effort to provide some guidance as to the effects of dynamic strain aging over the temperature range 275 to 400°C, a number of low-strain-rate fatigue tests were conducted. Results from these tests conducted at 371°C for several strain rates are shown in Fig. 10. Continuous cycling as well as tests with compressive hold times were conducted. The compressive hold time tests were run at a strain rate of 4×10^{-3}/sec during the ramp portion of the cycle. Then, for the overall cycle including the hold periods shown for strain ranges of 1 and 0.5%, the strain rates were 5.48×10^{-5} and 2.6×10^{-4}/sec, respectively. The tests conducted with compressive hold times given above failed after about the

same number of cycles as those tests conducted in continuous cycling at nearly corresponding strain rates, indicating perhaps that wave form was not important. The authors recommend that for applications involving low-strain-rate fatigue (i.e., considerably less than 4×10^{-3}/sec) where dynamic strain aging is a possiblity, the 427°C design curve be modified according to the reduction indicated in Fig. 10.

Tests are currently under way over the range 427 to 593°C to define the extent to which strain-controlled fatigue properties are adversely influenced by strain rate and hold or dwell periods at given values of strain. Edmunds and White (11) clearly demonstrated that the strain-controlled fatigue resistance of this material at 593°C was reduced by hold times and that the reduction increased with decreasing strain range. Manson et al. (12) showed that at this same temperature the amount of reduction in strain-controlled fatigue life for a given hold time depended upon the type of hold time (i.e., tension, compression, or both) with compressive hold times being the most damaging at lower strain ranges. In Fig. 11 continuous cycle fully reversed fatigue data are compared with 538°C test data that contained a tension, compression, or both a tension and compression hold time during each cycle for the duration indicated. The preliminary data are plotted as a diagram of time to failure versus cycles to failure (t-N) so that the reader might easily compare the fatigue life of a test that contained a given hold time for each cycle with the results of a zero hold time or continuous cycle test. Although creep-fatigue testing on this material is still in progress, some preliminary conclusions are possible from Fig. 11. Consistent with the conclusion reported from previous investigations (11, 12) for a given hold time the magnitude of the reduction in fatigue life increases with decreasing strain range ($\Delta\varepsilon_t$). Compressive holds are more damaging than tensile holds, but again the difference depends upon strain range, with greater differences occurring at lower strain ranges. Test information available at

both 482 and 427°C is consistent also with these tentative conclusions. The magnitude of the reduction in fatigue life attributed to the hold time effect, which probably results from both creep and environmental interaction, is greater at 538 and 482°C than at 427°C.

Cyclic crack growth tests using a Wedge Opening Load (WOL) specimen geometry and concepts of linear elastic fracture mechanics for treating the data have also been accomplished on this material. Figure 12 compares results from a number of tests conducted from room temperature to 593°C at several frequencies. Consistent with the results of the strain-controlled fatigue tests, crack growth rates (da/dn) or incremental change in crack length per cycle increased with increasing temperature. All the crack growth data were obtained from tension-tension tests, with the ratio of minimum to maximum load expressed as R. The data indicate only a small frequency effect over the range 40 to 300 cycles/min at 510°C. The data of Johnson (13) are also included in Fig. 12 for comparison; they were obtained on the same heat and heat treatment of 2 1/4 Cr-1 Mo steel that was used by ORNL (8), but with a 204-sec hold period at peak load each cycle. At 593°C there was a more pronounced frequency effect over the range 4 to 40 cycles/min; decreasing frequency resulted again in an increase in crack growth rates as shown. Above the knee in the curve for the elevated-temperature data shown in Fig. 12 the data can be represented by an equation of the form:

$$\frac{da}{dn} = A\,\Delta K^n \,, \tag{10}$$

where A and n are constants for a given temperature, R ratio, and frequency. Values of these constants are listed in Table IV.

Few of the components of reactor systems manufactured from this material and subject to cyclic loading will operate at zero mean stress. Therefore, mean stress effects must be accounted for, and R ratio studies were conducted.

The results of a number of tests at 510°C are shown in Fig. 13. Since frequency effects at 510°C are important, only those data at similar test frequencies are reported. The summary line for $R = 0.05$ at higher frequency is shown for comparison. The rate of crack growth increases markedly with increasing mean stress.

The data were reanalyzed with the concept of effective stress intensity factor used by Walker (14). The effective stress intensity factor, K_{eff}, is given by

$$K_{eff} = K_{max}(1 - R)^m \quad , \tag{11}$$

where m varies with the material. Using a value of $m = 0.5$ gave the results shown to the right in Fig. 13. The varying growth rates above the knee were effectively consolidated into a single line. However, the lower rates below the knee of the curve were not.

Above the knee in the curve the equation of the line is as follows:

$$\frac{da}{dn} = 3.852 \times 10^{-15}(K_{eff})2.17 \tag{12}$$

where K_{eff} is again in units of psi in.$^{1/2}$.

PHYSICAL PROPERTIES

The physical properties that are most important for the design of the LMFBR steam generators are the coefficient of thermal expansion, the thermal conductivity (λ) and the thermal diffusivity (D). Most of the material presented here has been covered in much more detailed fashion elsewhere, and, with the exception of some new material on λ, this section is largely a condensation of the earlier work (15). In presenting this synopsis, the intention is to emphasize (1) the values that we currently believe are the most appropriate for design, (2) the technical rationale for the choices, and

(3) the amount of variability that might reasonably be expected. The three properties are discussed separately below.

Thermal Expansion

The thermal expansion behavior of a material may be described in several different ways by (1) tabulating the percentage change in length as a function of temperature or (2) tabulating values for the slope of the length-temperature curve (instantaneous expansion coefficient) or (3) giving values of the linear slope required to generate the length change observed at each temperature. These quantities are all interrelated, and discussion is therefore limited to the third method of describing the length change data, which is commonly called the mean coefficient of expansion, α_M.

In a ferromagnetic alloy, existing theoretical treatments are known to be inadequate, and the expansion behavior must be obtained from experimental data. Unfortunately, experimental data are frequently subject to systematic errors. For example, the α_M data (16) on pure iron show a range of 6% at room temperature and 11% at 600°C. Somewhat less scattered, 4 and 8%, exists in the three sets of data (17–19) for 2 1/4 Cr-1 Mo steel, but this spread shows the danger inherent in relying on any one set of measurements.

The α_m estimates due to McElroy (15) are shown in Table V. These values were obtained by using Kirby's (16) values for pure iron, α_M (Fe) and developing an empirical equation involving a temperature- and concentration-dependent correction term. A best value for the constant was obtained by use of experimental data for several low-alloy steels (19–21), and the result was

$$\alpha_M = \alpha_M(\text{Fe}) - 0.075\left(\frac{T + 327}{600}\right) X \qquad (13)$$

where: T is temperature in K, X is total concentration of all solutes expressed in atomic percent, and α_M and α_M(Fe) are in units of 10^{-6}/K.

Since the value of the constant, 0.075, was determined by the deviation of experimental data for steels from Kirby's values for pure iron, the estimate really does not rely heavily on the uncertain α_M(Fe) values The obvious disadvantages of this approach are (1) it treats all solutes equally, (2) it is purely empirical, and (3) a temperature dependence is forced upon the data. Despite these difficulties, the equation is in reasonably good agreement with the 3 sets of data for 2 1/4 Cr-1 Mo, but favors the data of Fink et al. (19).

An obvious advantage of this approach is that Eq. (13) can be used to estimate how heat-to-heat composition variations will alter the expansion behavior. For 2 1/4 Cr-1 Mo, the allowable composition ranges correspond to a variation in total solute concentration of about 2.6 at. %. Using this result with the empirical equation results in an estimate that heat-to-heat variations could affect α_M by 1.8% at room temperature and 2.8% at 600°C. Also, since the best currently attainable measurements are probably accurate to about ±1%, designers should bear in mind that the expansion behavior cannot be determined to better than about ±2.5% at 600°C.

The α_M values that are shown in Table V were believed to be within about ±4% of the true values. In Fig. 14 the α_M values are compared with the ASME Code (22), and the difference is seen to be about −1.5% at all temperatures. This agreement, though encouraging, probably indicates that the ASME Code is primarily based on the data of Fink et al. (19). The ±4% uncertainty assigned to the Oak Ridge National Laboratory values still seems reasonable, since at 600°C the three sets of data spread by ±4%, compositional variations could contribute ±1.4%, and the experimental uncertainties associated with the particular measurements were probably larger than ±1%.

Thermal Conductivity

In the LMFBR heat exchanger, the heat transfer coefficients are very high, and conduction through the tube walls contributes a large part of the steady-state temperature drop between the two fluids. Further, in alloys the thermal conductivity, λ, is sensitive to small variations in microstructure and composition. Therefore, designers must have available detailed information on the magnitude and variability of λ.

The ORNL estimates for 2 1/4 Cr-1 Mo were based on (1) a small amount of accurate lower temperature (25–100°C) data and (2) the results of some earlier work (23) on mechanisms of the thermal conduction in pure iron. The method used for analyzing and extrapolating the λ data is somewhat complex, but a summary is useful because it illustrates how a band of λ values was obtained and shows how the complex temperature dependence of λ arises.

In an optically opaque solid, energy can be carried by the conduction electrons and by the lattice vibrations or phonons. Both Copper and BeO are good thermal conductors, yet, they represent limiting cases in which energy is transported by essentially only one mechanism. In transition metals, such as iron, the conduction electrons are scattered more strongly than in copper, and the electrical resistivity, ρ is much higher. In this situation, significant amounts of energy can be transmitted by the parallel conduction of the lattice vibrations and the behavior becomes complicated:

$$\lambda = \lambda_e + \lambda_p \ , \tag{14}$$

where λ_e = thermal conductivity due to conduction electrons, and

λ_p = thermal conductivity due to lattice vibrations.

In general, the two terms do not have the same temperature dependence. In non-ferromagnetic metallic elements, experiments show that λ_e rises to a peak at very low temperatures and then decreases to a nearly constant value at high

temperatures. Also, at high temperatures the Wiedemann-Franz-Lorenz law is approximately valid so that

$$\lambda_e = \frac{LT}{\rho} , \tag{15}$$

where L = a constant at high temperaures.

Since ρ of simple metals is proportional to T, the λ should remain essentially constant at high temperatures. Both theory and experiment (24) indicate that the thermal conduction from lattice vibrations dies away as the temperature is increased

$$\lambda_p \propto T^{-1} .$$

Thus, in a case where both λ_p and λ_e are significant at room temperature, λ_e is expected to dominate at high temperatures.

This simple picture does not account for the complex temperature dependence derived for 2 1/4 Cr-1 Mo steel. In this material, the λ first increases with T, reaches a mixmum in the vicinity of 300 to 400 K, and then decreases at higher temperatures. The high-temperature decrease is due to the loss of ferromagnetism which causes the ρ to rise much faster than T (25), and thus both λ_e and λ_p decrease in this range. This explanation holds for both iron and low-alloy steels. At lower temperatures, the measurements indicate a positive λ temperature coefficient, a situation observed for many alloys. This is explained by assuming that the alloying elements increase the scattering (ρ) by a large roughly temperature independent amount, A, and the magnetic disorder ρ is unimportant at lower temperatures. Then, involving the Wiedemann-Franz-Lorenz law:

$$\lambda_e = LT/(A + BT) . \tag{16}$$

For 2 1/4 Cr-1 Mo Steel (15), A is about 15 to 20 μΩ-cm and B is approximately 0.045 μΩ-cm K^{-1}. Thus λ_e is small at low temperature, but increases with increasing temperature. The computational model used in obtaining the ORNL λ values is somewhat more complex, and includes a term to account for the effects of chromium and molybdenum in solid solution on the λ_p of iron, separate Weidman-Franz values (Lorenz numbers) for the impurity and intrinsic ρ contributions and three constants derived from a treatment of data on high-purity iron (23).

This approach has several advantages: (1) it is consistent with existing theory, (2) the constants involved are derived from reliable experimental λ and ρ data, (3) it can account for the complex temperature dependence observed, and (4) heat-to-heat variations can be estimated through variations in ρ.

The minimum range for λ was generated in this way. Electrical resistivity data on several heats and for several heat treatment conditions were used in the extrapolated equation:

$$\lambda = \left[\frac{\rho - \rho_{Fe}}{L_0 T} + \frac{\rho_{Fe}}{1.002\, L_0\, [1 - \exp(-T/195 + 0.214)]T}\right]^{-1} + \left[\frac{T}{73} + 1.364 \times 10^5 (\rho - \rho_{Fe})_{298K}\right]^{-1} \quad (17)$$

where ρ = electrical resistivity of the 2 1/4 Cr-1 Mo Steel at T, Ω-cm;

T = temperature, K;

ρ_{Fe} = electrical resistivity of high purity at T, Ω-cm;

$L_0 = 2.443 \times 10^{-8}$ V^2/K^2;

$(\rho - \rho_{Fe})_{298\ K}$ = electrical resistivity values at 298 K, Ω-cm.

This generated a range of λ values, which was based on the variability in available ρ measurements.

Current work at ORNL involves further testing and refinement of the values that are shown in Table V. Lower temperature (26–100°C) λ and ρ data are being obtained on annealed material from nine commercial heats of 2 1/4 Cr-1 Mo Steel, and in a later phase of the work high-temperature λ data will be obtained on

two or three of these heats. The first λ results from this work on four heats fall within the upper half of the scatter band and show the predicted temperature dependence.

Thermal Diffusivity

This property is important for analyzing heat exchanger behavior during transients, and is related to the thermal conductivity:

$$D = \lambda / dC_p \tag{18}$$

where D = thermal diffusivity,

d = density, and

C_p = specific heat capacity.

However, physically, D is more complicated than λ since it is determined by the ability of the material to absorb energy as well as the carrier concentrations and mobilities. At present, direct D measurements have not attained the accuracy that can be achieved in λ experiments, and the best D data are usually good to about ±5%. The ORNL D values, which are shown in Table V and compared with the ASME code values in Fig. 14, were calculated from Eq. (18) using estimated d and C_p values and the λ values from Table V. The variability quoted includes additional contributions from uncertainties in the specific heat and density values (15) but is principally due to anticipated λ variations. It is interesting to note that the D estimates are in good (3–7%) agreement with the data of Fink et al. (19) for a steel (No. 6) that lies within the 2 1/4 Cr-1 Mo composition range, and the α_M data on this steel were also in good agreement with the ORNL estimates. As can be seen from Fig. 14, the ASME code values fall consistently below the ORNL estimates, as was the case for the λ results.

CONCLUSIONS

Much information defining the physical and mechanical properties of 2 1/4 Cr-1 Mo steel for steam generator design has recently become available. Although elevated-temperature behavior of this material is complicated by variables such as composition, heat treatment, thermomechanical processing, and temperature- and strain-rate-related effects; for annealed material tensile and creep behavior can be satisfactorily represented by empirical equations. Interim correlations for subcritical crack growth fatigue and creep-fatigue data were given to show progress in quantifying behavior under cyclic loading conditions. Key physical properties for steam generator design including thermal expansion, conductivity, and diffusivity were described in detail and compared with ASME Code values. presently accepted ASME Code values. The new thermal conductivity and diffusivity values were found to be significantly higher than the ASME Code values in the temperature range of interest for LMFBR heat exchanger applications.

ACKNOWLEDGMENTS

The authors gratefully thank R. T. King and S. Peterson for reviewing and editing the manuscript and Julia Bishop for typing the final document.

REFERENCES

1. W. E. Ray, S. L. Schrock, S. H. Shiels, and K. C. Thomas, "Selection of Steam Generator Tubing Material for the Westinghouse LMFBR Demonstration Plant." *Nuclear Technol.*, 29, 222 (1971).
2. S. L. Goodstine and J. L. Kurpen, "Corrosion and Corrosion Product Control in the Utility Boiler-Turbine Cycle." *Combustion*, 6, May, 1973.
3. M. K. Booker, T. L. Hebble, D. O. Hobson, and C. R. Brinkman, "Mechanical Property Correlations for 2 1/4 Cr-1 Mo Steel in Support of Nuclear Reactor Systems Design." presented at 3rd International Conferenence in Reactor Technology, Imperial College, London, Sept. 1–5, 1975. Submitted to *An International Journal of Pressure Vessels and Piping*, Applied Science Pub. Ltd. Essex, England.
4. R. L. Klueh and T. L. Hebble, "A Mathmatical Description for the Stress-Strain Behavior of Annealed 2 1/4 Cr-1 Mo Steel," Oak Ridge National Laboratory, Oak Ridge, Tennessee, report in preparation.
5. R. L. Klueh and R. E. Oaks, Jr., *High-Strain-Rate Tensile Properties of Annealed 2 1/4 Cr-1 Mo Steel*, Oak Ridge National Laboratory, Oak Ridge, Tennessee, report in preparation.
6. E. Voce, "The Relationship Between Stress and Strain for Homogeneous Deformation, *J. Inst. Met.*, 74: 537–62 (September 1948).
7. G. V. Smith, *Supplemental Report on the Elevated-Temperature Properties of Chormium-Molybdenum Steels (An Evaluation of 2 1/4 Cr-1 Mo Steel)*, ASTM Data Series Publication DS 6S2, American Society for Testing and Materials, Philadelphia, (1971).
8. C. R. Brinkman, M. K. Booker, J. F. Strizak, W. R. Corwin, J. L. Frazier, and J. M. Leitnaker, "Interim Report on the Continuous Cycling Elevated Temperature Fatigue and Subcritical Crack Growth Behavior of 2 1/4 Cr-1 Mo

Steel," Oak Ridge National Laboratory, Oak Ridge, Tennessee, report in preparation.

9. C. R. Brinkman, K. F. Booker, J. P. Strizak, and W. R. Corwin, "Elevated Temperature Fatigue Behavior of 2 1/4 Cr-1 Mo Steel," ASME Paper No., KB-19 PVP, presented at the Second National Congress on Pressure Vessels and Piping, San Francisco, Calif., June 23 to 27, 1975 of the American Society of Mechanical Engineers.

10. B. K. Langer, "Design of Pressure Vessels for Low-Cycle Fatigue," *J. Basic Eng.*, 84, 389–402 (1962).

11. H. G. Edmunds and D. J. White, "Observation of the Effect of Creep Relaxation on High-Strain Fatigue," *J. Mech. Eng. Sci.*, 8: (3), pp. 310–321, (1966).

12. S. S. Manson, G. R. Halford, and M. H. Hirschberg, "Creep-Fatigue Analysis by Strain Range Partitioning," NASA-TM-67838, Lewis Research Center, Cleveland, Ohio (1971).

13. R. G. Johnson, Department of Aerospace Engineering, Mechanical Engineering, and Engineering Mechanics, University of Alabama, private communication, July 1974.

14. E. K. Walker, "An Effective Strain Concept for Crack Propagation and Fatigue Life with Specific Applications to Biaxial Stress Fatigue," p. 225 in *Proc. Air Force Conf. on Fatigue and Fracture of Aircraft Structures and Materials*, H. A. Wood et al., eds., AFFDL-TR-70-144 (1970).

15. D. L. McElroy, "Estimated Physical Properties of 2 1/4 Cr-1 Mo Steel," Oak Ridge National Laboratory, Oak Ridge, Tennessee; report in preparation.

16. Private communication, R. K. Kirby, physicist, Length Section, Metrology Division, National Bureau of Standards to Professor C. R. Brooks, Chemical and Metallurgical Engineering Department, University of Tennessee, June 10, 1969.

17. R. Michel, "Elastic Constants and Coefficients of Thermal Expansion of Piping Materials Propsed for 1954 Code for Pressure Piping," *Trans. ASME*, 77, 151–59 (1955).

18. J. Motz, 55, 489 (1964), attributed to Technical Data of Mannesmann AG, Dusseldorf, and the Phoeniz-Rhein rohr AG, Dusseldorf.

19. V. K. Fink, F. Richter, U. Lotter, and K. Schrecke, *Thyssenforschung* 2, 65 (1970).

20. The British Iron and Steel Research Association, ed., *Physical Constants of Some Commercial Steels at Elevated Temperatures* (based on measurements made at the National Physical Laboratory, Teddington) Butterworths Scientific Publications, London (1953).

21. J. L. Everhart, W. E. Lindlief, J. Kanegis, P. G. Weissler, and F. Siegel, "Mechanical Properties of Metals and Alloys," Circular C447, National Bureau of Standards (1943).

22. *Summer 1974 Addenda Section III-Division 1 Nuclear Plant Components, ASME Boiler and Pressure Vessel Code*, The American Society of Mechanical Engineers, pp. 103–104.

23. R. K. Williams and W. Fulkerson, "Separation of the Electronic and Lattice contributions and to the Thermal Conductivity of Metals and Alloys." 398–456 in *Thermal Conductivity Proceedings of the Eighth Conference*, ed. by C. Y. Ho and R. E. Taylor, Plenum Press, New York (1969).

24. P. G. Klemens, "Thermal Conductivity and Lattice Vibrational Modes" in *Solid State Physics Advances in Research Applications*, Vol. 7 pp. 1–98, ed. by F. Seitz and D. Turnbull, Academic Press, Inc., New York, (1958).

25. W. Fulkerson, J. P. Moore, and D. L. McElroy, "Comparison of the Thermal Conductivity, Electrical Resistivity, and Seebeck Coefficient of High-Purity Iron and an Armco Iron to 1000°C, *J. Appl. Phys.* 37: (7) 2639–2653, (June 1966).

Figure Captions

Fig. 1. Three-dimensional representation of yield strength as a function of temperature and strain rate.

Fig. 2. Three-dimensional representation of ultimate tensile strength as a function of temperature and strain rate.

Fig. 3. Three-dimensional representation of total elongation as a function of temperature and strain rate.

Fig. 4. Three-dimensional represenation of the reduction in area with temperature and strain rate.

Fig. 5. The variation of A_4 of the Voce equation with temperature and strain rate.

Fig. 6. The variation of B_4 of the Voce equation with temperature and strain rate.

Fig. 7. The variation of C_4 of the Voce equation with temperature and strain rate.

Fig. 8. Expected value of Yield strength (0.2% Offset) with upper and lower tolerance limits.

Fig. 9. Proposed ASME design curves for 2 1/4 Cr-1 Mo steel in the annealed condition for temperatures indicated without mean stress corrections.

Fig. 10. Total strain range, $\Delta\varepsilon_t$, versus cycles to failure at 700°F (371°C), showing the influence of strain rate on the strain-controlled fatigue properties of 2 1/4 Cr-1 Mo steel.

Fig. 11. Time to failure versus cycles to failure diagram showing the influence of various hold periods on the strain-controlled cyclic lifetime of 2 1/4 Cr-1 Mo steel tested at 1000°F (538°C).

Fig. 12. Effect of temperature and frequency of fatigue crack propagation of 2 1/4 Cr-1 Mo steel.

Fig. 13. Effect of stress ratio on fatigue crack propagation of 2 1/4 Cr-1 Mo steel at 950°C (510°C) in air.

Fig. 14. Difference in physical property value as a function of temperature for 2 1/4 Cr-1 Mo steel.

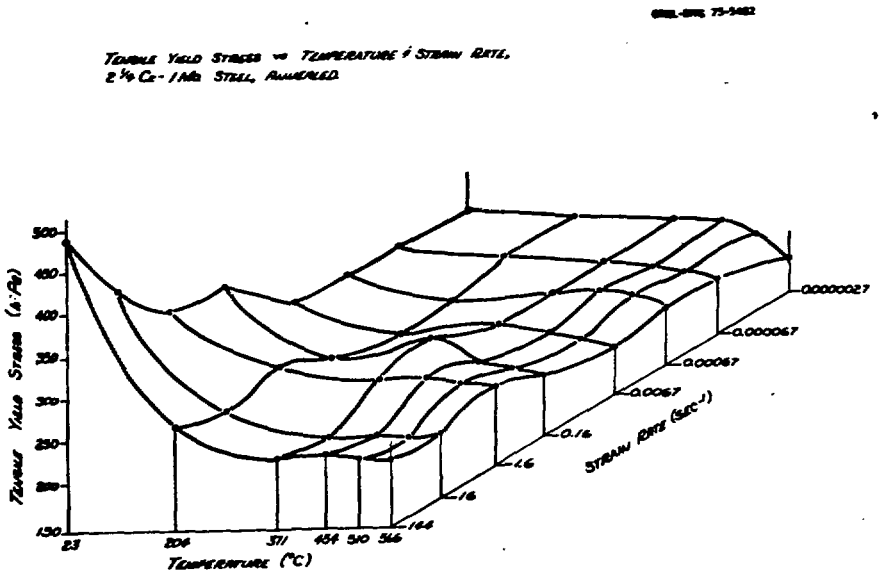

Figure 1. Three-Dimensional Representation of Yield Strength as a Function of Temperature and Strain Rate.

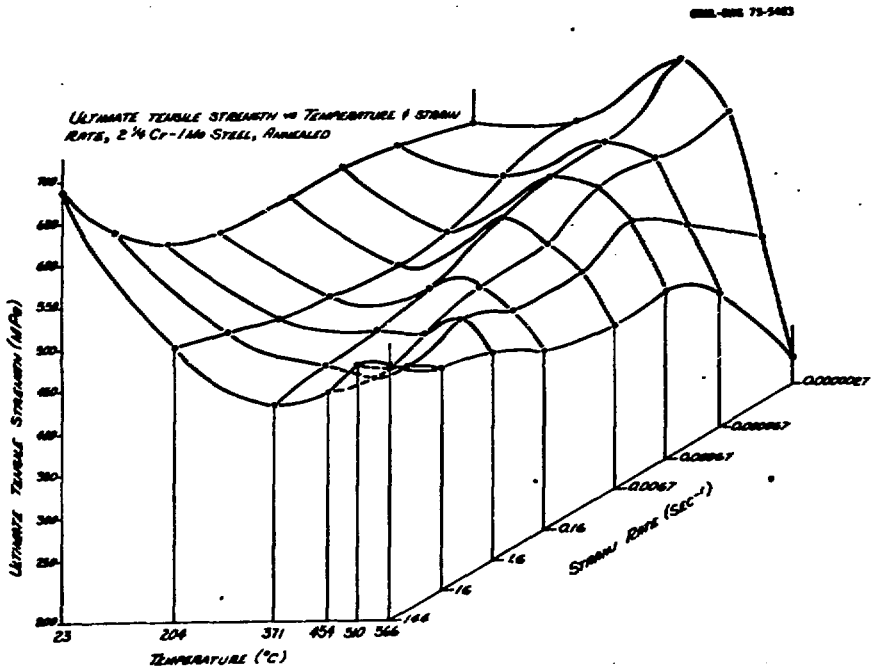

Figure 2. Three-Dimensional Representation of Ultimate Tensile Strength as a Function of Temperature and Strain Rate.

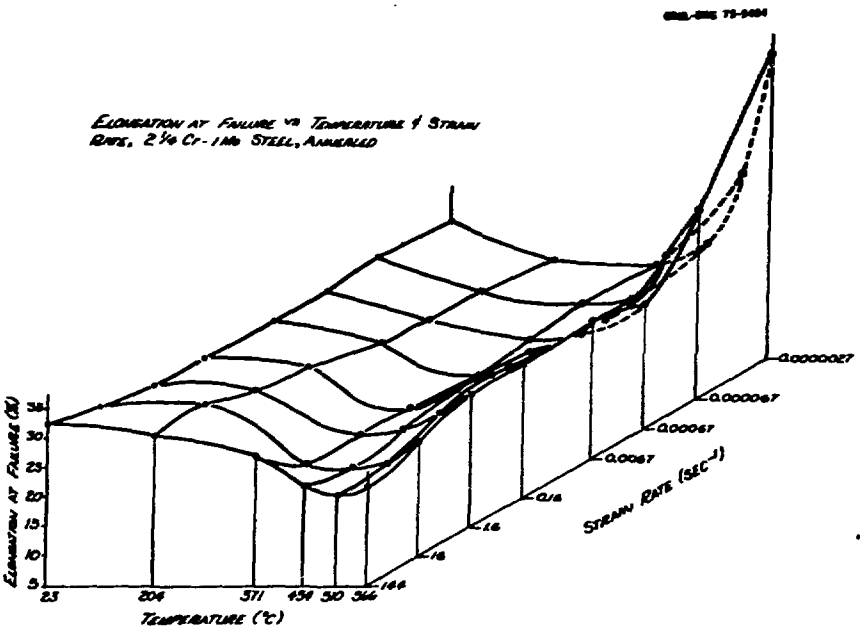

Figure 3. Three-Dimensional Representation of Total Elongation as a Function of Temperature and Strain Rate.

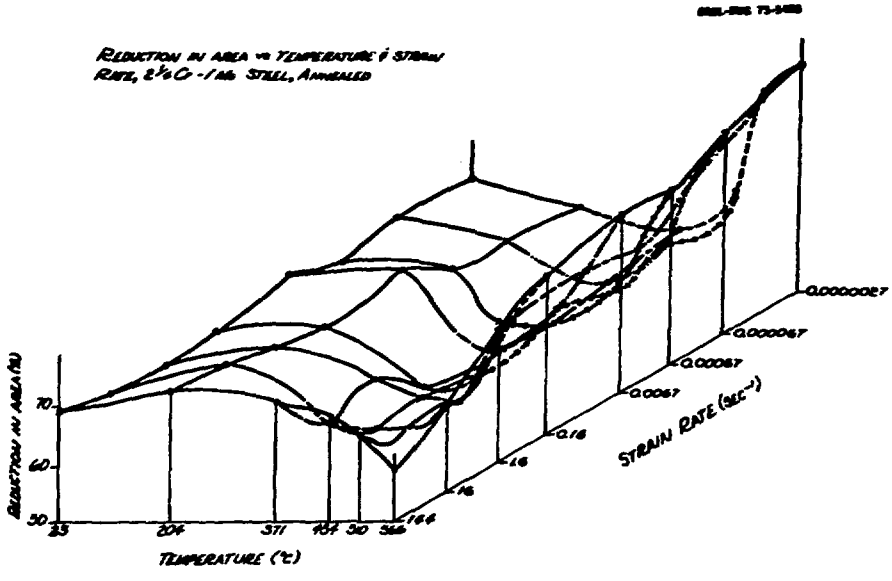

Figure 4. Three-Dimensional Representation of the Reduction in Area with Temperature and Strain Rate.

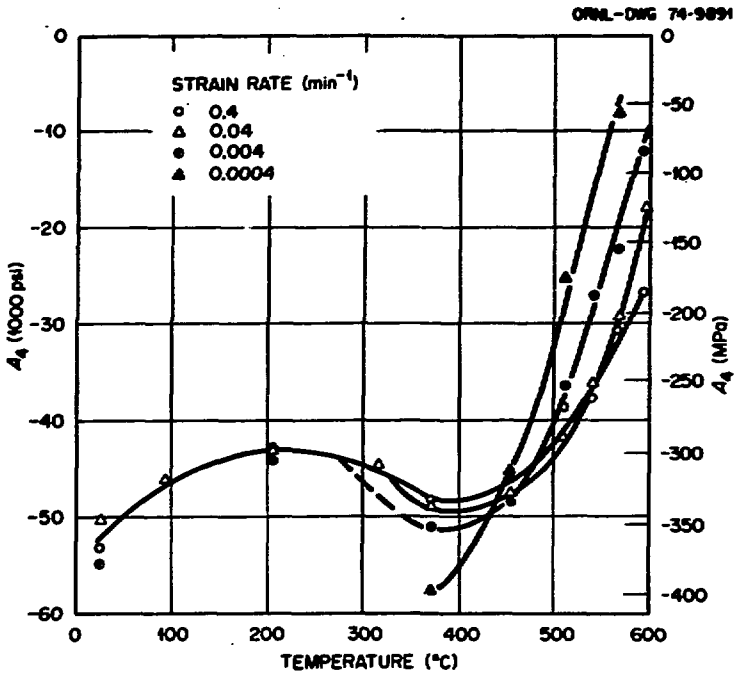

Figure 5. The Variation of A_4 of the Voce Equation with Temperature and Strain Rate.

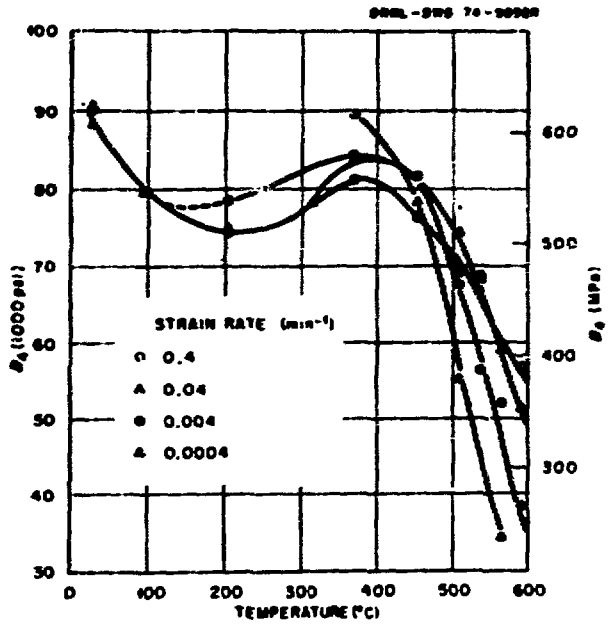

Figure 6. The Variation of B_4 of the Voce Equation with Temperature and Strain Rate.

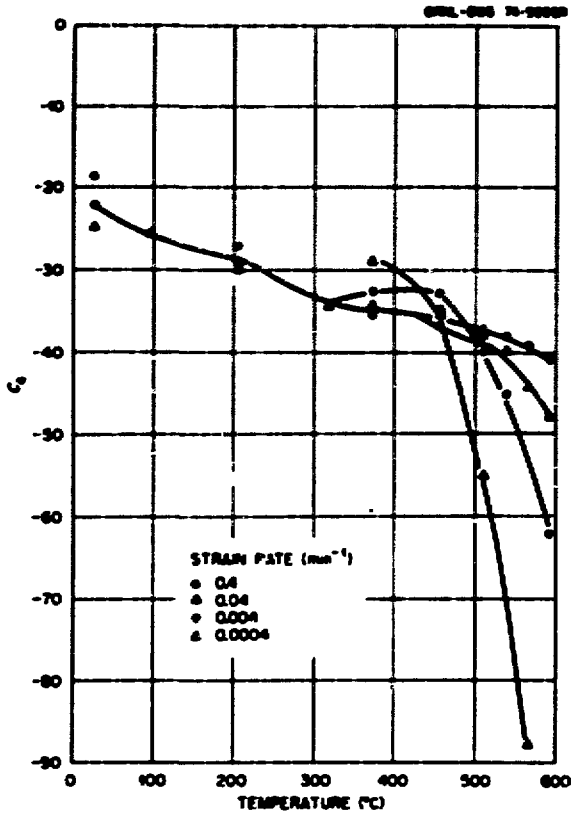

Figure 7. The Variation of C_4 of the Voce Equation with Temperature and Strain Rate.

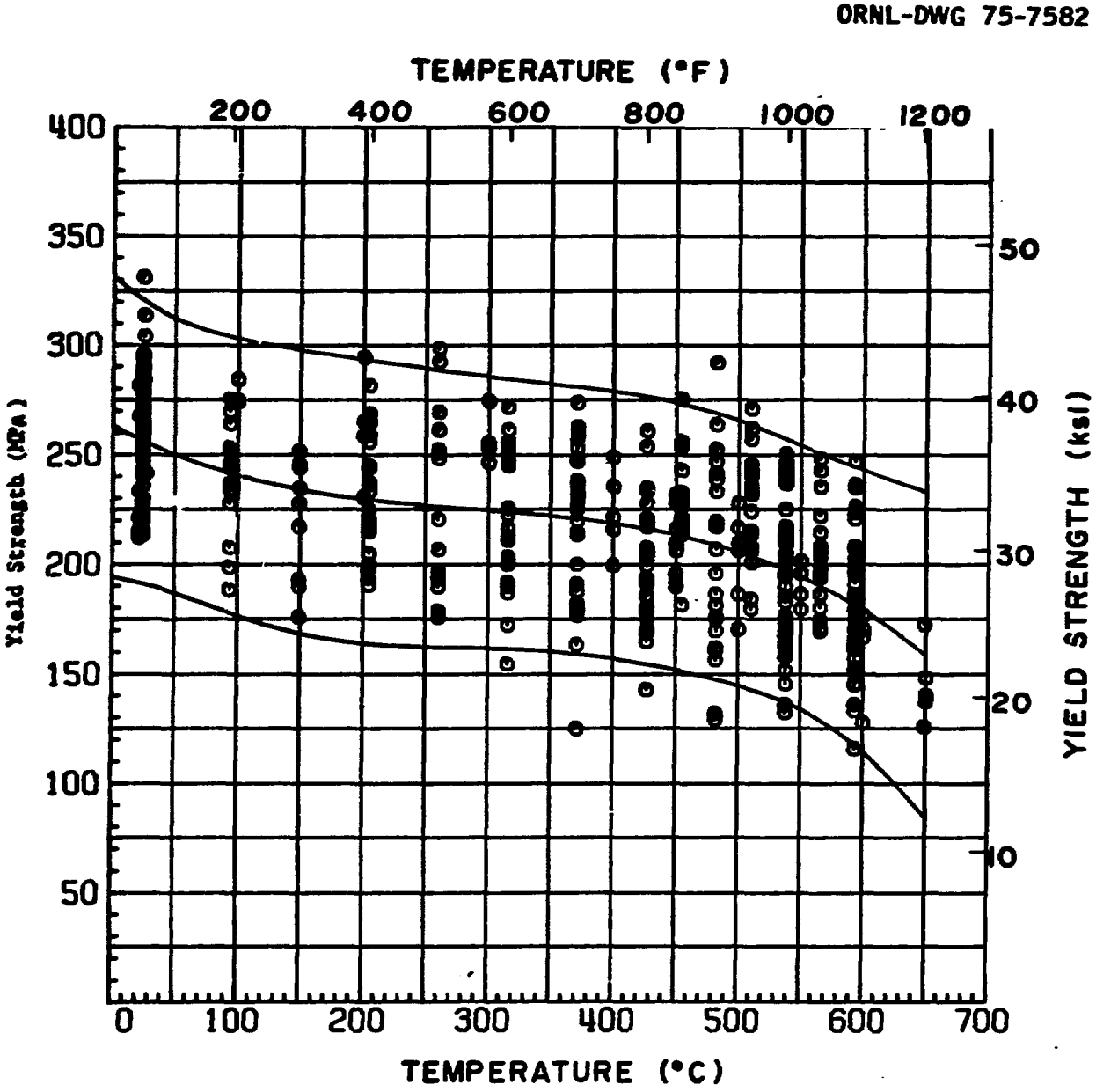

Figure 8. Expected Value of Yield Strength (0.2% Offset) With Upper and Lower Tolerance Limits.

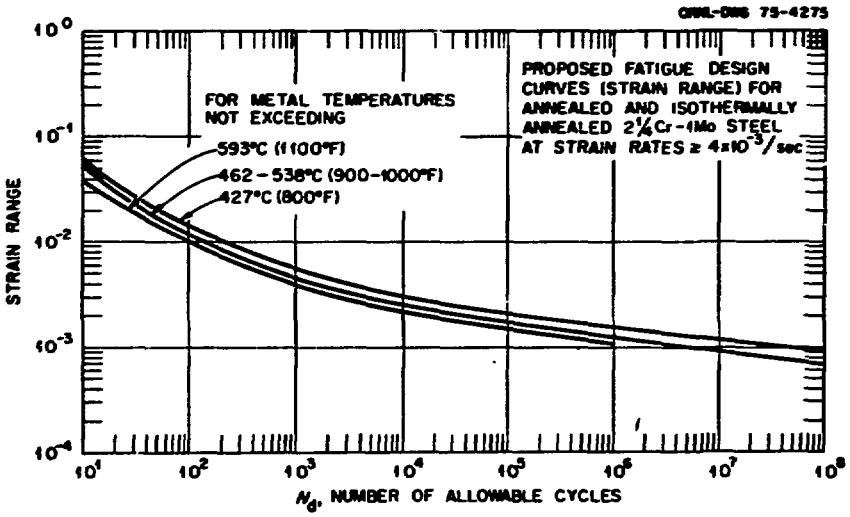

Figure 9. Proposed ASME Design Curves for 2 1/4 Cr-1 Mo Steel in the Annealed Condition for Temperatures Indicated Without Mean Stress Corrections.

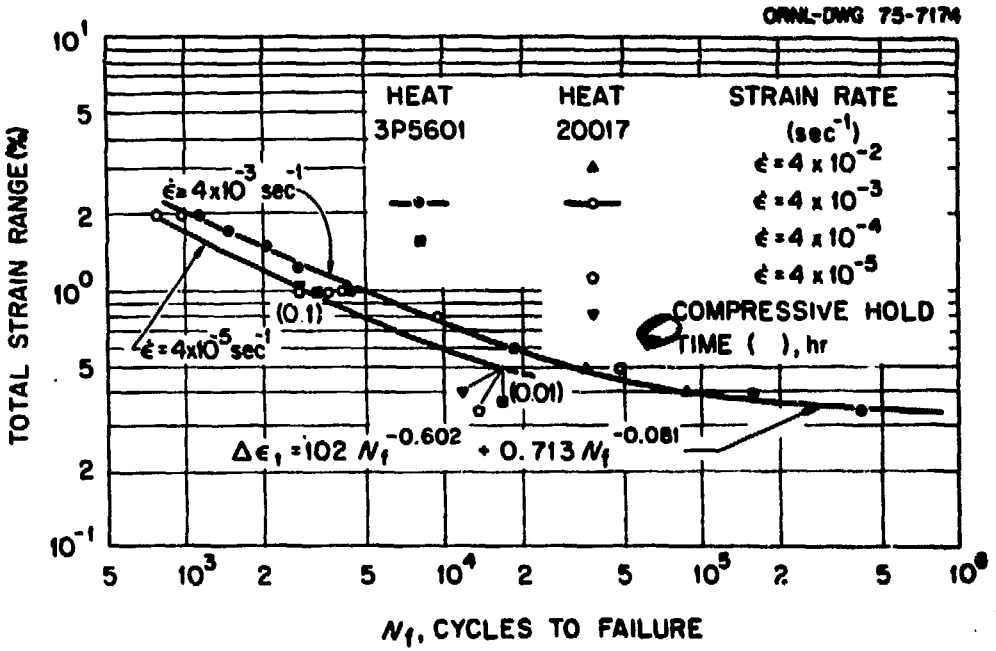

Figure 10. Total Strain Range, $\Delta\epsilon_t$, Versus Cycles to Failure at 700°F (371°C) showing the Influence of Strain Rate on the Strain Controlled Fatigue Properties of 2¼ Cr-1 Mo steel.

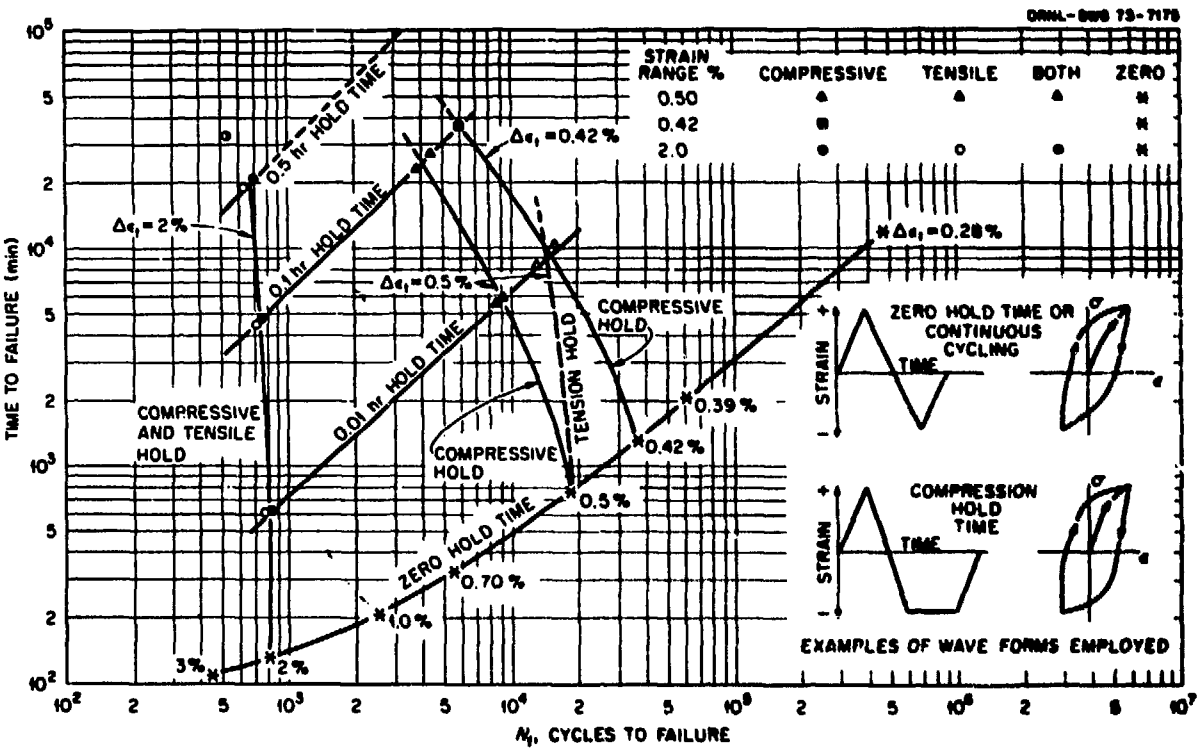

Figure 11. Time to Failure versus Cycles to Failure Diagram showing the Influence of Various Hold Periods on the Strain Controlled Cyclic Lifetime of 2¼ Cr-1 Mo Steel Tested at 1000°F (538°C).

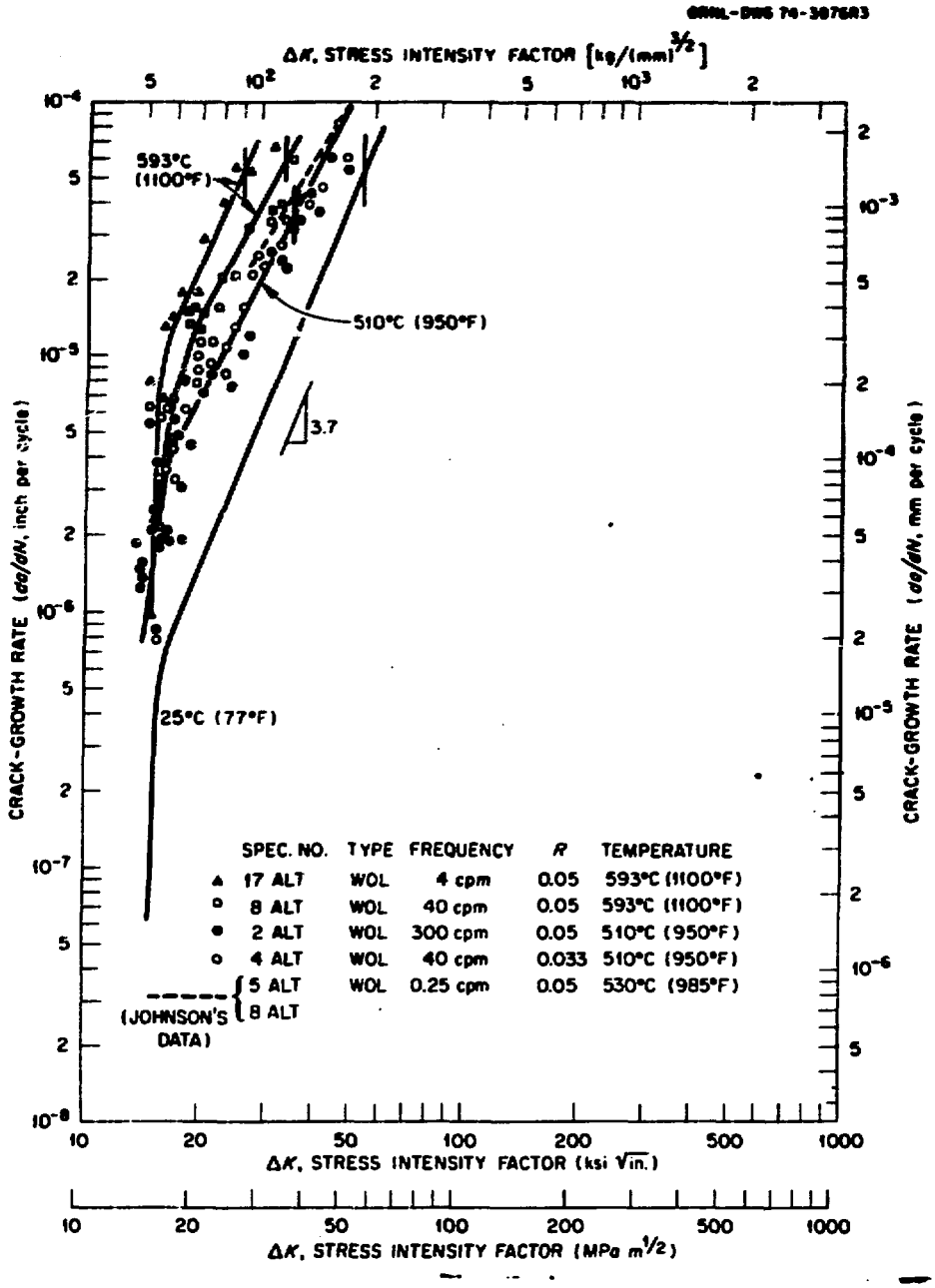

Figure 12. Effect of Temperature and Frequency on Fatigue Crack Propagation of 2¼ Cr-1 Mo Steel.

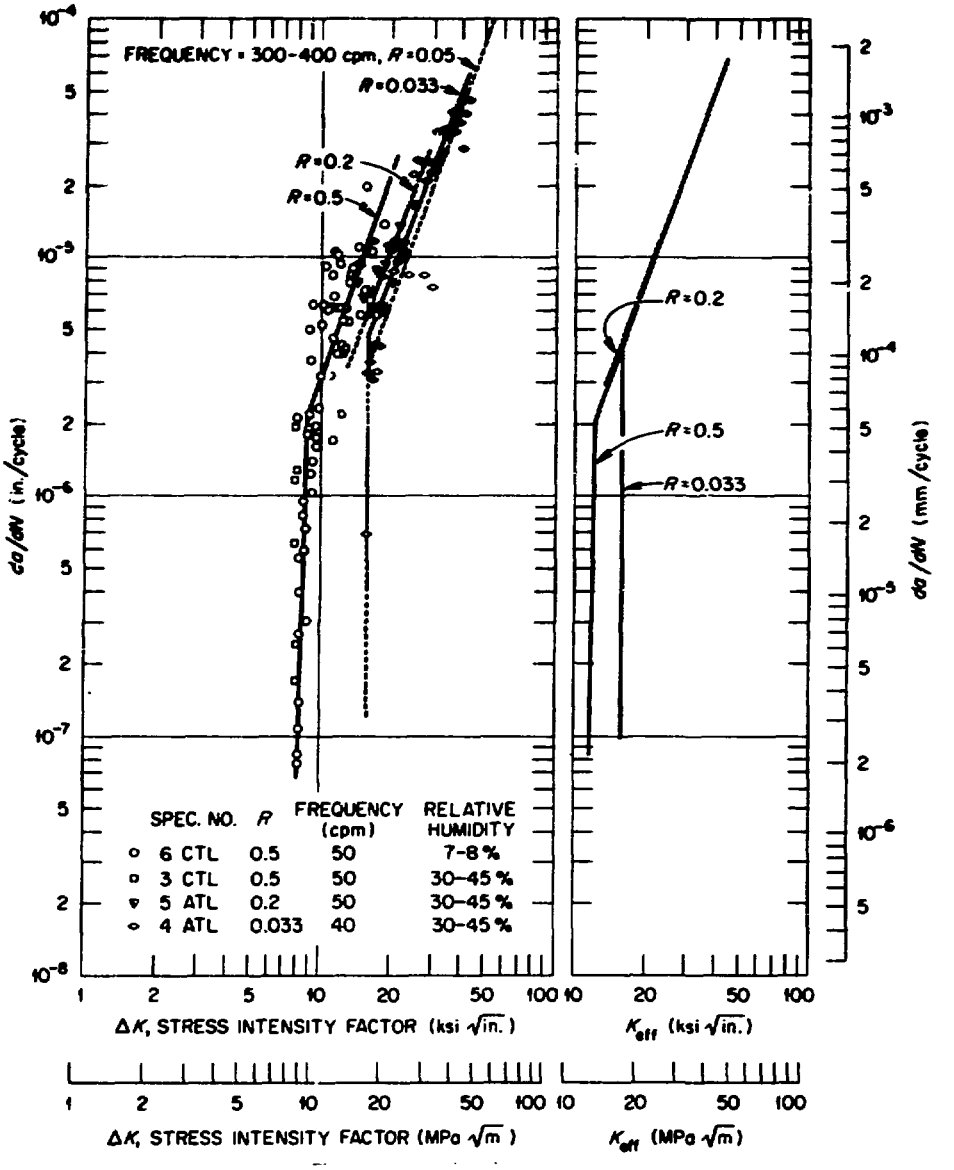

Figure 13. Effect of Stress Ratio on Fatigue-Crack Propagation of 2¼ Cr-1 Mo Steel at 950°F (510°C) in Air.

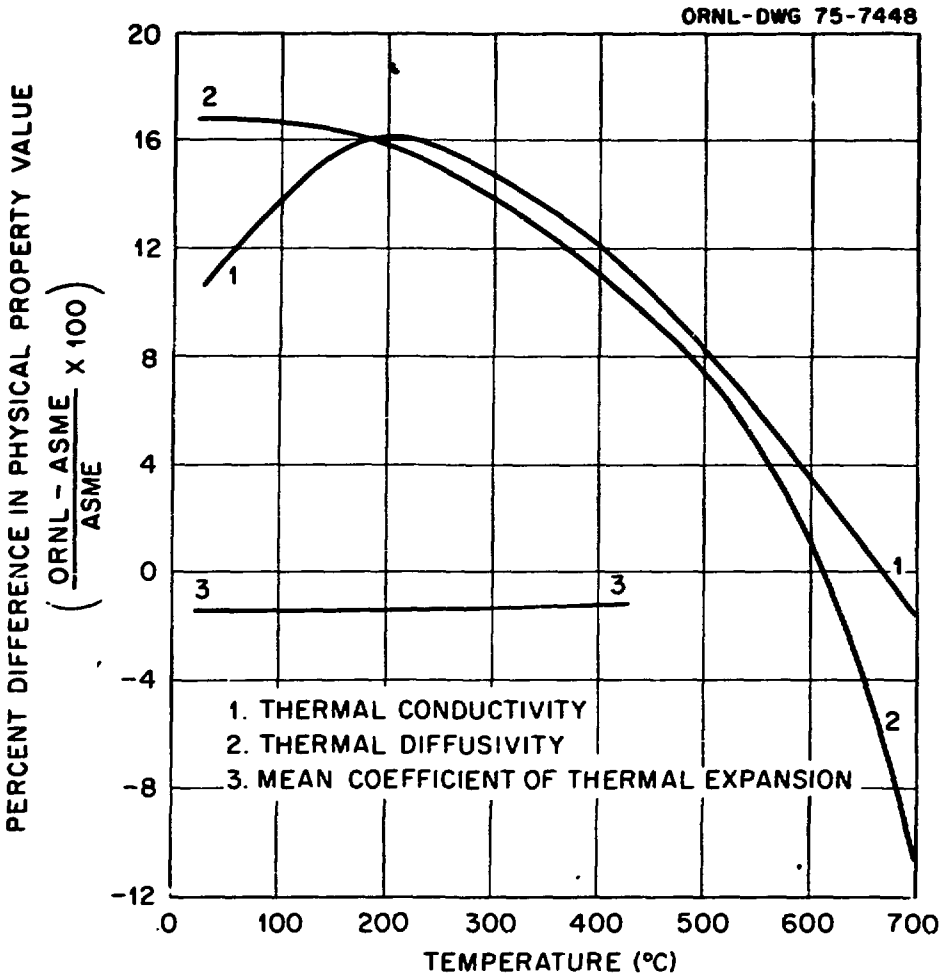

Figure 14. Difference in Physical Property Value as a Function of Temperature for 2 1/4 Cr-1 Mo Steel.

Table I

Partial Tabulation of Mechanical and Physical Property Tests Required in order to Establish Behavior of CRBRP Steam Generator Materials

I. Mechanical

- A. Monotonic and cyclic uniaxial tensile
- B. Constant-load uniaxial creep
- C. Friction and Wear
- D. Step- and reversed-load creep
- E. Cyclic Creep
- F. Elastic property
- G. Relaxation
- H. Complex Loading
- I. High-cycle and low-cycle fatigue
- J. Subcritical crack growth
- K. Toughness
- L. Creep-fatigue-environment interaction

II. Physical

- A. Thermal expansion
- B. Thermal conductivity
- C. Emittance
- D. Density
- E. Electrical resistivity
- F. Thermal diffusivity
- G. Specific heat

Table II

Chemical Composition of 25.4-mm (1-in.) Plate of Annealed 2 1/4 Cr-1 Mo Steel (B&W Heat 20017)

Analysis	Chemical Composition, wt %							
	C	Mn	Si	Cr	Mo	Ni	S	P
Vendor	0.11	0.55	0.29	2.13	0.90		0.014	0.011
ORNL	0.135	0.57	0.37	2.2	0.92	0.16	0.016	0.012

Table III

Coefficients of Equation for Predicting Onset of Teriary Creep in 2 1/4 Cr-1 Mo Steel

Coefficient	Value and Standard Error	
	SI Units (MPa and K)	English Units (ksi and °R)
b_0	12.05 ± 5.4	18.94 ± 1.7
b_1	−0.465 ± 1.6	−3.15 ± 0.57
b_2	−0.00759 ± 0.0037	−0.00805 ± 0.00083
b_3	−0.0389 ± 0.017	−0.00370 ± 0.0024

Table IV

Constants for $da/dn = A\ \Delta K^n$ for 2 1/4 Cr-1 Mo Steel

Temperature (°C)	R	Frequency (cycles/min)	Constants[a]	
			A	n
Room	0.05	40–4800	3.26×10^{-22}	3.65
510	0.05	40–300	2.47×10^{-15}	2.15
510	0.2	50	8.96×10^{-12}	1.41
510	0.5	50	9.95×10^{-15}	2.15
593	0.05	40	7.05×10^{-13}	1.72
593	0.05	4	3.14×10^{-14}	2.08

[a]For ΔK in psi(in.)$^{1/2}$.

Table V

Physical Property Estimates for 2 1/4 Cr–1 Mo Steel

Temperature (°C)	Thermal Conductivity		Thermal Diffusivity		Mean Coefficient of Thermal Expansion (deg^{-1})
	Value $W\ cm^{-1}\ K^{-1}$	Minimum Expected Variability ± %	Value (cm^2/sec)	Minimum Expected[a] Variability ± %	All Values ±4%
25	0.363	11	0.103	13	11.45×10^{-6}
100	0.370	10	0.0986	12	11.94
200	0.374	8	0.0926	11	12.53
300	0.366	7	0.0846	9	13.03
400	0.354	6	0.0759	8	13.46
500	0.338	4	0.0664	7	13.82
600	0.320	4	0.0557	6	14.10
700	0.302	3	0.0431	5	14.30

[a]Variation includes uncertainties in specific heat capacity, density, and thermal conductivity.